Physical Communication 28 (2018) 154–165

Contents lists available at ScienceDirect

Physical Communication

journal homepage: www.elsevier.com/locate/phycom

Full length article

Coexistence in fourth generation digital subscriber lines: Experiment, modeling, and simulation results

Sanda Drakulić, Martin Wolkerstorfer, Driton Statovci *

Institute of Telecommunications, TU Wien, Gußhausstraße 25/E389, A-1040 Vienna, Austria

ARTICLE INFO

Article history:
Received 22 October 2017
Received in revised form 2 March 2018
Accepted 4 April 2018
Available online 12 April 2018

Keywords:
Subscriber loops
Broadband communication
Intersymbol interference
DSL
G.fast
VDSL2

ABSTRACT

The deployment of fourth generation digital subscriber line (DSL) technology ("G.fast") will be gradual and it may therefore share the cable infrastructure with legacy DSL technologies such as Very high speed DSL transceivers 2 (VDSL2). We perform experiments on coexistence of G.fast with legacy VDSL2, highlighting the practical relevance of out-of-band leakage and aliasing. Furthermore, the differences in transmission parameters (e.g., carrier width and sampling rate) and asynchronous transmission results in inter-carrier and inter-symbol interference (ICSI). Previous work on modeling ICSI in the communication field focused on modeling only a subset of these effects. Hence, we analytically derive a simplified ICSI model, which notably includes the effects of aliasing, leakage, and worst-case symbol misalignment. Our results partially based on simulations show that a) neglecting ICSI potentially leads to significant bit-rate overestimation (e.g., 18% in G.fast rates); and b) a G.fast start frequency of approximately 23 MHz may provide sufficient spectral separation with VDSL2 profile 17a transceivers.

1. Introduction

Digital subscriber line (DSL) broadband access has been evolving from exclusively copper-based to hybrid fiber-copper deployments. Although fiber-to-the-home (FTTH) is superior to hybrid fiber-copper deployments in terms of achievable bit-rates, its deployment incurs additional costs compared to the reuse of existing copper infrastructure due to the digging of trenches and fiber installation. In [1] it is shown that hybrid architectures such as fiber-to-the-distribution-point (FTTdp) save up to 80% in investment compared to FTTH. Therefore, FTTdp represents an intermediate solution to enable fiber-like speeds over the copper network and to allow operators to spread fiber investments over a longer time period. The International Telecommunication Union (ITU) has released recommendations on fourth generation DSL, specifically tailored to FTTdp deployments, called G.fast [2,3]. It targets gigabit aggregate bit-rates (downstream + upstream) over loops of few hundred meters and utilizes frequencies up to 212 MHz. However, not all service operators and customers are expected to replace existing DSL systems, such as Very high speed DSL transceivers 2 (VDSL2), with G.fast. Therefore, the coexistence of G.fast and VDSL2 is a realistic scenario in future DSL access networks.

Crosstalk cancellation ("vectoring"), is a key feature of G.fast. Current vectoring schemes assume that the crosstalk signals among different tones are orthogonal to each other. Different G.fast and VDSL2 transmission parameters such as multiplexing schemes, tone spacings, and sampling rates, produce inter-carrier and inter-symbol interference (ICSI) which couples crosstalk signals between different tones and consequently makes joint per-tone vectoring among different technologies impractical. Therefore, G.fast supports a configurable start frequency [4,5], which enables spectral separation between different systems. As shown in [4,6], starting G.fast transmission immediately above VDSL2 may result in strong ICSI for both systems, cf. also our motivating testbed experiment results in Section 2. A large spectral separation on the other hand potentially incurs a significant performance penalty, especially for longer (e.g., >100 m long) G.fast loops. Therefore, in order to optimize the selection of the G.fast start frequency and to estimate the achievable bit-rates of coexisting G.fast and VDSL2 (e.g., for spectrum balancing), a performance model which captures ICSI along with the impact of receive and transmit filtering is required.

The problem of ICSI in asynchronous DSL systems with *identical transmission parameters* has been studied in [7,8]. A frequency-domain crosstalk cancelation model between *synchronous* VDSL2 systems with different tone spacing has been presented in [9]. The authors in [10] analyze coexistence of G.fast and VDSL2 taking far-end crosstalk (FEXT) and near-end crosstalk (NEXT) into account, but neglecting the effects of ICSI. The problem of ICSI due to time and frequency offsets has also been well studied in the wireless literature. Exemplary studies on ICSI in wireless field for

* Corresponding author.
E-mail addresses: sanda.drakulic@nt.tuwien.ac.at (S. Drakulić), martin.wolkerstorfer@nt.tuwien.ac.at (M. Wolkerstorfer), driton.statovci@nt.tuwien.ac.at (D. Statovci).

https://doi.org/10.1016/j.phycom.2018.04.002

ideal and time-variant channels can be found in [11–15] while the authors in [16,17] address ICSI due to the joint effects of carrier and sampling frequency offsets. Models of ICSI produced jointly by frequency and time variations have been studied in [18–22]. However, all these ICSI models do not take differences in transmission parameters such as tone spacings and sampling rates into account, motivating the development of a simple model of coexistence in DSL.

Preliminary results related to this work have appeared in [23] and were later applied to spectrum balancing in [24]. Our main novel contributions are (a) the definition of a reworked and extended ICSI model for asynchronous discrete multitone (DMT) systems with different tone spacing and sampling rate (significantly improved and more realistic compared to that in [23]) where the model is not only restricted to DSL but it can also be used for interference analysis in other multi-carrier networks[1] ; (b) we include detailed derivations of crosstalk gains under ICSI, the influence of realistic receive and transmit filters, and the verification by time-domain simulations; and (c) an extensive simulation study on the exemplary application of the model in the selection of the G.fast start frequency and VDSL2 filtering for G.fast/VDSL2 (profile 17a) coexistence.[2]

The paper is organized as follows. In Section 2 we present motivating experiment results on VDSL2/G.fast coexistence, showing the potential out-of-band leakage as well as aliasing observed using off-the-shelf DSL equipment. In Section 3 we review DMT system models with and without ICSI from literature. Afterwards we turn to the derivation and analysis of a novel ICSI model for asynchronous multicarrier systems capturing also transmission differences and the influence of filtering. Additionally, we derived an upper bound on ICSI gains. Furthermore, Section 3.3 includes the verification of the proposed ICSI model by time-domain simulations. A specific application of the developed ICSI model to the problem of selecting the G.fast start-frequency for coexistence with VDSL2 is studied in Section 4 while conclusions of our work are drawn in Section 5.

2. Motivation: VDSL2/G.fast coexistence

In order to motivate this work on modeling the coexistence of different DSL technologies, we conducted experiments on a testbed using commercial DSL equipment (VDSL2 and G.fast DSL access multiplexers/DSLAMs; G.fast modems as well as three different types of VDSL2 modems). The cabling is realized by laying (shielded or unshielded) drop cables of 30-130 m length in isolated ducts (cf. the schematic illustration in Fig. 1(a)), using actual phone sockets on the line-termination side (denoted by "0A" — "5D" in Fig. 1(a)) and (30-pair) quad installation cables/patch panels on the network-termination side. NEXT from VDSL2 was measured at the connection point (i.e., close to the disturbers' DSLAM) using a spectrum analyzer (connected through a North Hills 50 Ω/124 Ω Balun; terminating the unused end of the measured line) under the disturbance of 22 non-vectored VDSL2 lines (bandplan 998/ADE17-M2x). This measurement was also qualitatively confirmed (results omitted) through readings of the actual G.fast quiet-line noise (QLN) from a G.fast victim line using its management interface [25]. Furthermore, we read the upstream and downstream QLN perceived by a VDSL2 line under disturbance from 13 G.fast lines. These disturbers include the line connected through the same quad as the victim line as well as all remaining "unshielded" drop

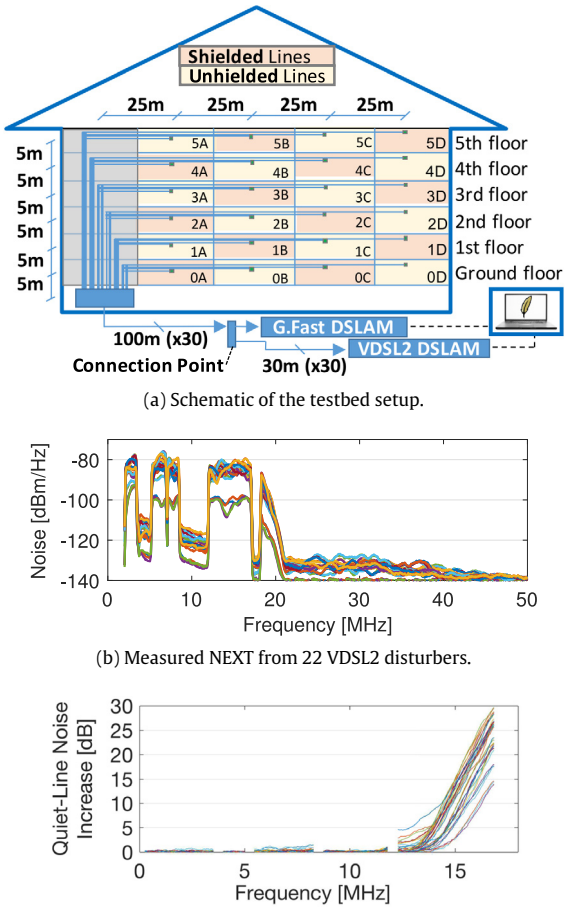

(a) Schematic of the testbed setup.

(b) Measured NEXT from 22 VDSL2 disturbers.

(c) VDSL2 QLN increase caused by *spectrally separated* G.fast disturbers (i.e., "aliasing").

Fig. 1. Testbed setup (a), results on measured near-end crosstalk (NEXT) from 22 VDSL2 disturbers (b), and perceived VDSL2 crosstalk quiet-line noise (QLN) from 13 spectrally separated G.fast disturbers due to aliasing reported on three different VDSL2 modem types (c).

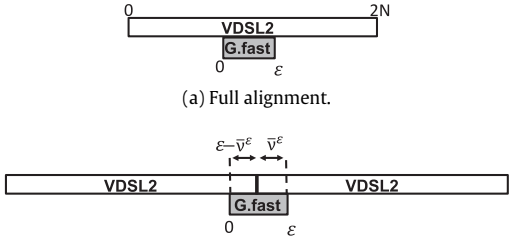

(a) Full alignment.

(b) Partial alignment.

Fig. 2. Possible time alignments between VDSL2 and G.fast for a G.fast DFT block size of ε samples and symbol offset $\bar{\nu}^{\varepsilon}$.

lines, and we configured G.fast profile 106a and switched off tones below 17.6 MHz as well as tones in the FM radio band (confirmed through spectrum analyzer measurements).[3] This implies tight spectral separation between the two DSL technologies. The latter

[1] DSL channels are usually static (i.e., *time-invariant*); therefore, the developed model only holds for time-invariant channels.

[2] Note that the selection of profile 17a is only exemplary and based on its pronounced relevance in practice. Similar studies could be performed using our model for other bandplans, such as the wider VDSL2 profile 35b.

[3] Note that due to the total power constraint of G.fast the notching of further frequency bands results in a reallocation of transmit power to lower frequencies (subject to the power spectral density mask) and therefore increases the observed disturbance from G.fast lines.

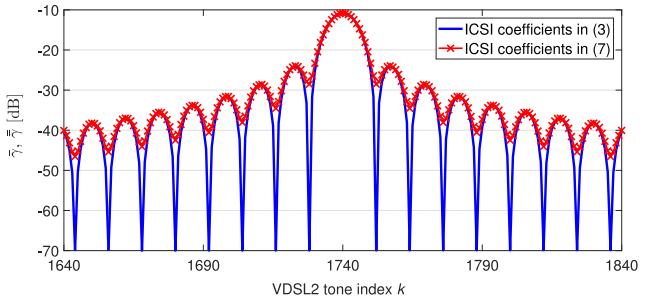

Fig. 3. Comparison of ICSI coefficients for G.fast tone $\bar{k} = 145$ calculated based on (3) (special case of full symbol alignment) and (7) (average of fully aligned and worst-case partially aligned symbols), respectively.

experiment was repeated under three different VDSL2 modem types.

The results illustrate the VDSL2 out-of-band leakage which harms G.fast when spectral separation is insufficient (cf. Fig. 1(b) where the NEXT falls below −130 dBm/Hz only above approximately 21 MHz) and the increased QLN due to aliasing seen by a VDSL2 line when G.fast is active right above the VDSL2 band (cf. Fig. 1(c)). Note that in the latter test we observed differences between the VDSL2 modem types, and we see that the aliasing noise is mostly restricted to the third downstream band (which is a consequence of different upstream frontends as described in Section 4.3). This would imply that the G.fast spectrum, *in this experimental setup (based on VDSL2 profile 17a)*, should be notched up to approximately 23 MHz.[4]

3. System and digital ICSI signal model

In the following we present our system model for synchronized discrete multitone (DMT) transmission with identical transmission parameters on all U transmitters. Furthermore, we show how this system model changes in case of nonidentical transmission parameters. We consider a DSL network with a set of users indexed by $\mathcal{U} = \{1, \ldots, U\}$ and a set of Δf [Hz] spaced tones indexed by $\mathcal{K} = \{1, \ldots, K\}$. The achievable bit-rate of user u on tone k is given by

$$b_k^u = \log_2\Big(1 + \frac{|h_k^u|^2 p_k^u}{\Gamma(\sum_{j\in\mathcal{U}\setminus u} |h_k^{u,j}|^2 p_k^j + \sigma_k^u)}\Big), \tag{1}$$

where Γ represents the signal-to-noise ratio gap to capacity, $h_k^{u,j}$ is the channel gain from user j to user u on tone k, and h_k^u is the direct channel gain of user u on tone k. The terms σ_k^u and p_k^u represent the background noise and transmit power spectral density (PSD) of user u on tone k, respectively. Under ICSI the achievable bit-rate of user u on tone k in (1) needs to be modified as [7]

$$\check{b}_k^u = \log_2\Big(1 + \frac{|h_k^u|^2 p_k^u}{\Gamma(\sum\limits_{j\in\mathcal{U}\setminus u}(\sum\limits_{\bar{k}\in\mathcal{K}} \gamma_{k,\bar{k}}^{u,j} |h_{\bar{k}}^{u,j}|^2 p_{\bar{k}}^j) + \sigma_k^u)}\Big), \tag{2}$$

where $\gamma_{k,\bar{k}}^{u,j}$ represents the ICSI coefficient from user j to user u, and from tone $\bar{k}$ to tone k, and $h_{\bar{k}}^{u,j}$ is the channel gain from user j to user u on G.fast tone $\bar{k}$. Note that the received ICSI depends on the PSD allocation of all users on all tones.

[4] More precisely, the last downstream band starts at 12 MHz and its first used tone at 12.29 MHz. Hence, we would notch the G.fast tones up to 17.66 + (17.66 − 12.29) = 23.04 MHz.

3.1. Influence of VDSL2 on G.fast

The derivation of a simplified model of the ICSI coefficients from a VDSL2 transceiver to a G.fast transceiver is based on the following intuitive steps. First we recognize that there are two main possible symbol alignment scenarios (full and partial alignment) as illustrated in Fig. 2. We model a VDSL2 transceiver in the digital domain by first calculating the inverse discrete Fourier transform (IDFT) of an "aligned" VDSL2 symbol. Assuming Nyquist sampling we applying M-times oversampling at the VDSL2 transmitter followed by low-pass (anti-imaging) filtering, where $M := \frac{\bar{f}_s}{f_s}$ and $\bar{f}_s$ and f_s are the sampling rates of G.fast and VDSL2, respectively ($\bar{f}_s > f_s$). Furthermore, VDSL2 and G.fast use different carrier spacings Δf and $\overline{\Delta f}$, where $\overline{\Delta f} > \Delta f$ and we define $L := \frac{\overline{\Delta f}}{\Delta f}$ which is assumed to be an integer value. The number of VDSL2 tones N and G.fast tones $\bar{N}$ are therefore related as $N = \frac{L\bar{N}}{M}$, i.e., $\frac{N}{L} = \frac{\bar{N}}{M}$. For example, the VDSL2 profile 17a and the G.fast profile 106a result in $L = 12$ and $M = 6$.

Next the transmitted symbol is filtered and convolved with the channel, resulting in distinguishable interference components from the positive and negative spectrum. Correspondingly we define the spacings $\bar{d}_1 = \frac{k}{L} - \bar{k}$ and $\bar{d}_2 = \frac{(2N-k)}{L} - \bar{k}$ between VDSL2 and G.fast tones k and $\bar{k}$. Lastly, power gains are derived as expected values, assuming user independence and equal reference impedances. Note also that $\frac{2N}{L}$ may not be an integer in general, which requires defining average ICSI coefficients over the varying discrete Fourier transform (DFT) block sizes in the model.

For full symbol alignment (cf. Fig. 2(a)), as derived in Appendix A.1, the average ICSI coefficients are calculated as

$$\bar{\gamma}(\bar{d}_1, \bar{d}_2) = \alpha\bar{\gamma}^{\varepsilon=\lfloor\frac{2N}{L}\rfloor}(\bar{d}_1, \bar{d}_2) + \beta\bar{\gamma}^{\varepsilon=\lceil\frac{2N}{L}\rceil}(\bar{d}_1, \bar{d}_2), \tag{3}$$

where $\alpha = \mathrm{mod}(\frac{2N}{L}, 1)$ and $\beta = 1 - \alpha$ are the fractions of symbols with length equal to $\lfloor\frac{2N}{L}\rfloor$ and $\lceil\frac{2N}{L}\rceil$, respectively. For overlapping tones the average ICSI $\bar{\gamma}(0, \bar{d}_2)$ is calculated as in (A.9) and analogously for $\bar{\gamma}(\bar{d}_1, 0)$.

The derivation under partial symbol alignment (cf. Fig. 2(b)) is similar, where we initially assume two independent VDSL2 symbols are truncated using a rectangular window. As derived in Appendix A.2, the average ICSI coefficients analogously to (3) are calculated as

$$\begin{aligned}\bar{\gamma}(\bar{d}_1, \bar{d}_2, \bar{\nu}^{\varepsilon=\lfloor\frac{2N}{L}\rfloor}, \bar{\nu}^{\varepsilon=\lceil\frac{2N}{L}\rceil}) \\ = \alpha\bar{\gamma}^{\varepsilon=\lfloor\frac{2N}{L}\rfloor}(\bar{d}_1, \bar{d}_2, \bar{\nu}^{\varepsilon=\lfloor\frac{2N}{L}\rfloor}) + \beta\bar{\gamma}^{\varepsilon=\lceil\frac{2N}{L}\rceil}(\bar{d}_1, \bar{d}_2, \bar{\nu}^{\varepsilon=\lceil\frac{2N}{L}\rceil}).\end{aligned} \tag{4}$$

As we see, these derived crosstalk coefficients depend on the symbol offset on the offset $\bar{\nu}^{\varepsilon}$, which in practice is not available. Therefore, a key contribution is the derivation of an analytical worst-case expression over possible symbol offsets. In the rest of the paper we consider a bound on the worst-case ICSI coefficients depending on the offset $\bar{\nu}^{*\varepsilon} = \mathrm{argmax}_{0\le\bar{\nu}^{\varepsilon}\le\varepsilon}\{f^{\varepsilon}(\bar{d}_i, \bar{\nu}^{\varepsilon})\}$. The analytic expression for $f(\bar{d}_i, \bar{\nu}^{*\varepsilon})$ is rigorously derived in Appendix B and the worst-case ICSI has the following form:

Proposition 1. *A bound on the worst-case* ICSI *coefficients in (4) is given by*

$$\bar{\gamma}^*(\bar{d}_1, \bar{d}_2) = \alpha\bar{\gamma}^{*\varepsilon=\lfloor\frac{2N}{L}\rfloor}(\bar{d}_1, \bar{d}_2) + \beta\bar{\gamma}^{*\varepsilon=\lceil\frac{2N}{L}\rceil}(\bar{d}_1, \bar{d}_2), \tag{5}$$

where $\bar{\gamma}^{*\varepsilon}(\bar{d}_1, \bar{d}_2) = \frac{\bar{Q}_{\bar{k}}^2 H_{\bar{k}}^2}{(\frac{2N}{L})^2 L}(\bar{\rho}^*(\bar{d}_1) + \bar{\rho}^*(\bar{d}_2))$, *where*

$$\bar{\rho}^*(\bar{d}_i) = \begin{cases} \dfrac{f^{*\varepsilon}(\bar{d}_1)}{\sin^2(\frac{\pi L\bar{d}_1}{2N})}, & \text{for } |\bar{d}_i| \neq 0, \\ \varepsilon^2, & \text{for } |\bar{d}_i| = 0, \end{cases}$$

and where

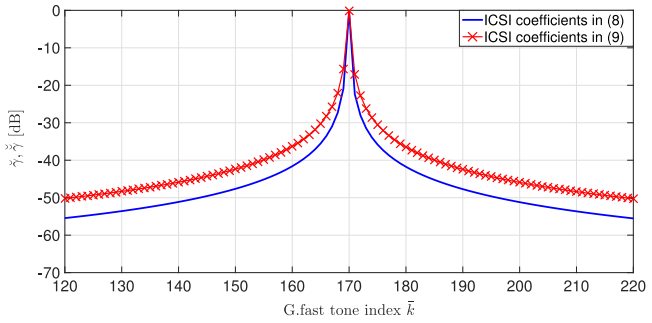

Fig. 4. ICSI coefficients for VDSL2 tone $k = 2039$ calculated with (8) (synchronous transmission) and (9) (weighted average with worst-case symbol offsets), respectively.

$$f^{*\varepsilon}(\bar{d}_i) = \max_{0\le\bar{v}^{\varepsilon}\le\varepsilon} \{f^{\varepsilon}(\bar{d}_i, \bar{v}^{\varepsilon})\} \tag{6a}$$

$$= \begin{cases} \sin^2(\frac{\pi L\bar{d}_i}{2N}\varepsilon), & \text{if } 0 < (\frac{\pi L|\bar{d}_i|}{2N}) < \frac{\pi}{2}, \\ 2\sin^2(\frac{\pi L\bar{d}_i}{4N}\varepsilon), & \text{if } \frac{\pi}{2} < (\frac{\pi L|\bar{d}_i|}{2N}) \bmod 2 < \frac{3\pi}{2}, \\ 2\cos^2(\frac{\pi L\bar{d}_i}{4N}\varepsilon), & \text{if } 0 \le (\frac{\pi L|\bar{d}_i|}{2N}) \bmod 2 < \frac{\pi}{2}, \\ & \text{or } \frac{3\pi}{2} < (\frac{\pi L|\bar{d}_i|}{2N}) \bmod 2 < 2\pi, \\ 1, & \text{if } |\bar{d}_i| = F\frac{2N}{L}\varepsilon^{-1} \\ & \text{where } F \text{ is uneven integer.} \end{cases} \tag{6b}$$

Proof. The proof is given in Appendix B. □

Finally, average ICSI coefficients for partial symbol alignment are obtained by taking into consideration $(L-1)$ aligned VDSL2 symbols and two partially aligned VDSL2 symbols, i.e.,

$$\bar{\tilde{\gamma}}(\bar{d}_1, \bar{d}_2) = \frac{(L-1)}{L}\bar{\gamma}(\bar{d}_1, \bar{d}_2) + \frac{1}{L}\bar{\gamma}^*(\bar{d}_1, \bar{d}_2), \tag{7}$$

where $\bar{\gamma}(\bar{d}_1, \bar{d}_2)$ (the contribution of fully aligned symbols) and $\bar{\gamma}^*(\bar{d}_1, \bar{d}_2)$ (the worst-case contribution of partially aligned symbols) are defined in (3) and (5), respectively. A comparison of ICSI coefficients using Eqs. (3) and (7) corresponding to symbol alignment and weighted average coefficients with worst-case symbol offset, respectively, on G.fast tone $\bar{k} = 145$ is shown in Fig. 3.[5]

We note that the derivations above involve two key approximations. Firstly, we have assumed that the ICSI coefficients are neither user nor tone dependent (see also the discussion in [8]). Hence, the derived ICSI coefficients are a function of the tone spacing between interfering and victim tone only. Secondly, the model has been simplified by neglecting the impact of the cyclic prefix between consecutive symbols.

3.2. Influence of G.fast on VDSL2

The derivation of the ICSI gain from a G.fast system to VDSL2 follows similar arguments, approximations, and methodology as presented in Section 3.1. For L fully aligned G.fast symbols, i.e., it is corresponding to synchronous transmission, as derived in Appendix C, the average ICSI coefficients are calculated as

$$\breve{\gamma}(d_1, d_2) = L\tilde{\gamma}(d_1, d_2), \tag{8}$$

where $\tilde{\gamma}(d_1, d_2)$ is defined as in (C.3). For partial alignment, $L-1$ fully aligned and two worst-case aligned G.fast symbols, the average ICSI coefficients are calculated as

$$\breve{\tilde{\gamma}}(d_1, d_2) = (L-1)\tilde{\gamma}(d_1, d_2) + \tilde{\gamma}^*(d_1, d_2), \tag{9}$$

where $\tilde{\gamma}(d_1, d_2)$ and $\tilde{\gamma}^*(d_1, d_2)$ are defined as in (C.3) and (C.5), respectively.

An exemplary comparison of per-symbol ICSI coefficients calculated using (8) and (9) for VDSL2 tone $k = 2039$ is shown in Fig. 4.[6]

3.3. Verification of the ICSI model

The analytical ICSI models described in Sections 3.1 and 3.2 are verified by simulations of a simple signal chain, consisting of an IDFT/scaling, a transmit filter, resampling/time shifting, receive

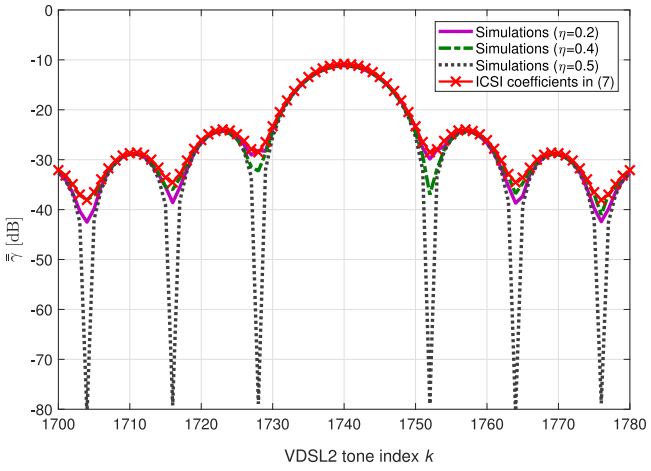

Fig. 5. Comparison of simulations with different relative symbol-shifts η and the upper bound on ICSI coefficients in (7) for G.fast victim tone $\bar{k} = 145$.

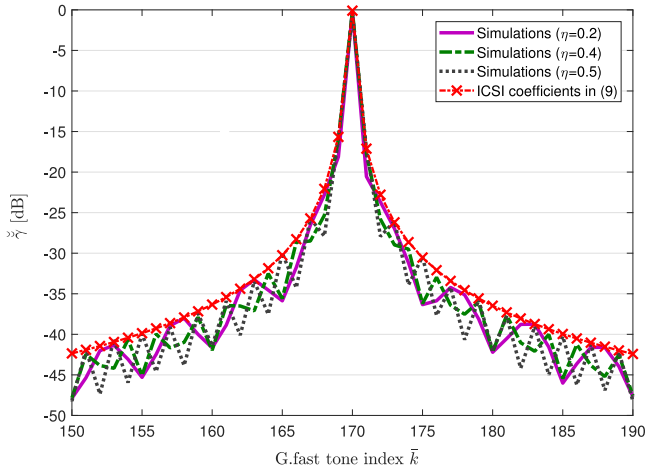

Fig. 6. Comparison of simulations with different relative symbol-shifts η and the upper bound on ICSI coefficients in (9) for VDSL2 victim tone $k = 2039$.

[5] Simulation parameters selected as in Section 4 and assuming perfect VDSL2 transmit-filtering.

[6] Simulation parameters selected as in Section 4 and assuming perfect VDSL2 receive-filtering.

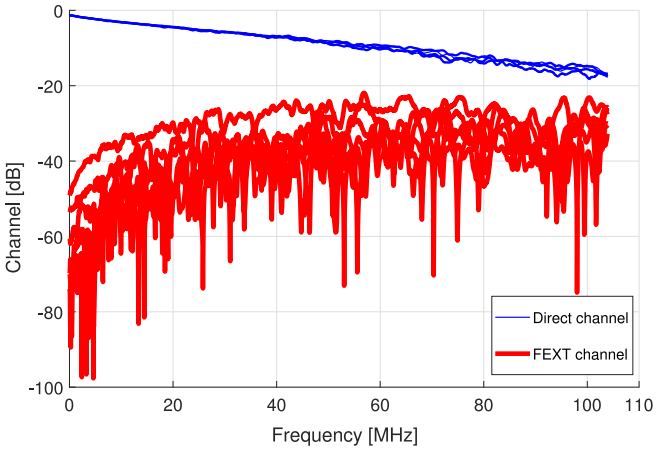

Fig. 7. Direct and FEXT channel gains used in simulations scaled to 50 m loop length.

filter, and an DFT/rescaling. An exemplary comparison between analytical ICSI model and signal-level simulations is provided in Figs. 5 and 6 from which we see that the derived per-tone bounds in (7) and (9) are fairly tight.

4. Simulation results

4.1. Simulation environment

We consider Chebyshev type I filters (motivated by [26]) with different orders ($r = 6$ or 8) and 0.5 dB passband ripple at VDSL2 transceivers while no filtering is simulated at G.fast transceivers. Note that G.fast filtering cannot eliminate the spectral images of VDSL2 and therefore does not have any influence on our simulation results. We also assume the same 17.7 MHz cut-off frequency for both upstream and downstream VDSL2 transmission. The simulation assumptions also include a flat background noise of -140 dBm/Hz, PSD masks according to [27] (VDSL2, profile 17a,and bandplan B8-11) and [2] (G.fast, profile 106a), an SNR gap of 10.75 dB, and an upstream/downstream asymmetry ratio for G.fast of 1:4. G.fast and VDSL2 use 4 dBm and 14.5 dBm per-line sum transmit power, respectively. The values of $\overline{\Delta f}$ and Δf are equal to 51.75 kHz and 4.3125 kHz, respectively, and therefore we have $M = 6$ and $L = 12$. Furthermore, due to the different duplexing techniques used in VDSL2 and G.fast (frequency division duplexing and time division duplexing) the crosstalk is composed of FEXT and NEXT. We use measured direct-channel and FEXT data of an underground cable of 100 m length, cf. Fig. 7. FEXT channel gains are nonlinearly scaled to various loop lengths based on the common empirical FEXT model in [28, Eq.(3.4)]. In addition we use a common conservative European NEXT coupling model [28] for calculating NEXT gains (which is appropriate to obtain worst-case bit-rates under interference from/to VDSL2). In all our simulations we use the spectrum balancing algorithm described in [24].

A mixed G.fast and VDSL2 topology is assumed, where the distance l_1 between VDSL2 DSLAM and G.fast distribution point unit (DPU) varies from 0 m to 500 m and the distance l_2 between G.fast DPU and customer premises equipment (CPE) side varies from 50 m to 200 m, cf. Fig. 8. All U lines are in a single cable binder, with the number of VDSL2 and G.fast users being equal to $U_{\text{VDSL2}} = U_{\text{G.fast}} = 4$, being co-located at the CPE side. In this work we aim at a conservative estimate of the losses in bit-rates due to coexistence of VDSL2 and G.fast, respectively. Therefore, all presented results in the upcoming analyses are based on our worst-case asynchronous ICSI models in (7) and (9).

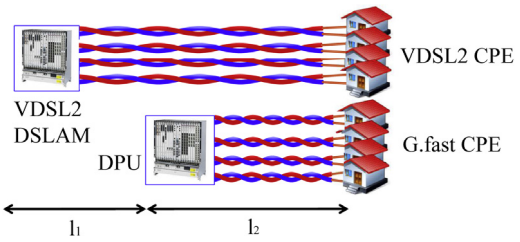

Fig. 8. Simulated network topology.

4.2. Model comparison with and without ICSI

In this Section we compare our ICSI model under transmit filtering with results obtained under the model in [10], which accounts for inter-group FEXT and NEXT but does not account for the influence of ICSI. In the following analysis VDSL2 and G.fast share the spectrum between 2.2 MHz and 17.67 MHz, i.e., there is no spectral separation between these two systems. Simulation results indicate that the largest gap between these two models in estimated mutual interference occurs for low order filtering (e.g., $r = 6$) and topologies where VDSL2 and G.fast users are collocated on both ends. This gap further increases, especially for G.fast users, for higher values of l_2, i.e., longer (FEXT) coupling lengths. In Fig. 9 we show the total VDSL2 and G.fast downstream noise (i.e., FEXT, NEXT and background noise) estimated with our ICSI model under Chebyshev type I filtering, perfect filtering, and with the ICSI-free model in [10]. We simulate a network scenario where users are collocated on both ends (i.e., $l_1 = 0$ m) and $l_2 = 200$ m.

Our ICSI model under *perfect filtering* and the model in [10] yield approximately the same noise levels for both VDSL2 and G.fast. A notable exception are VDSL2 frequencies below 2.2 MHz since the model in [10] omits the ICSI influence while due to the absence of G.fast receive-filtering noise leakage (i.e., ICSI) from higher frequencies occurs in case of VDSL2 perfect filtering. Furthermore, the ICSI estimated with the model in [10] disappears for G.fast frequencies above 17.67 MHz while our ICSI model results in substantial noise leakage above 17.67 MHz caused by (filtered) VDSL2 spectral images/leakage. Similarly, our ICSI model results in higher noise than the model in [10] for VDSL2 frequencies between approximately 12 MHz and 17.67 MHz due to the aliased G.fast frequencies. Note however, that the difference in estimated noise between the two models is higher for G.fast than for VDSL2 due to the higher VDSL2 downstream transmit PSD. This is also reflected in the achievable bit-rates where our simulations show that the model in [10] overestimates the average G.fast and VDSL2 downstream bit-rates by approximately 18% and 7%, respectively, compared to our ICSI model under lower order filtering ($r = 6$), $l_1 = 0\,m$, and $l_2 = 200\,m$. For higher order filtering (i.e., $r \geq 8$) the gap in estimated noise and in achievable bit-rates between these two models diminishes. The same conclusions can also be drawn for upstream transmissions.

4.3. Application example: Selection of a G.fast start frequency for coexistence with VDSL2

We analyze the spectral separation between G.fast and VDSL2/17a required to reduce interference between these two technologies to a negligible level. We exemplarily consider two G.fast start frequencies (f_{start}): 18 MHz ("tight" spectral separation) and 23 MHz (as indicated in our experiment results due to aliasing into the third downstream band). We start by analyzing the influence of G.fast on VDSL2. Fig. 10 shows the noise levels at the

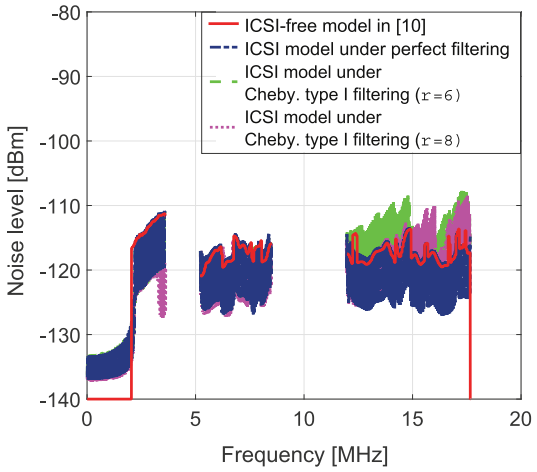

(a) Total VDSL2 noise.

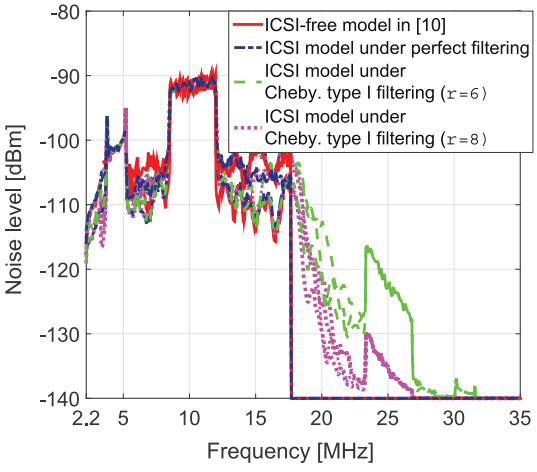

(b) Total G.fast downstream noise.

Fig. 9. Total VDSL2/G.fast noise estimated with our ICSI model under different types of filtering, and with ICSI-free model in [10] ($l_1 = 0$ and $l_2 = 200$ m).

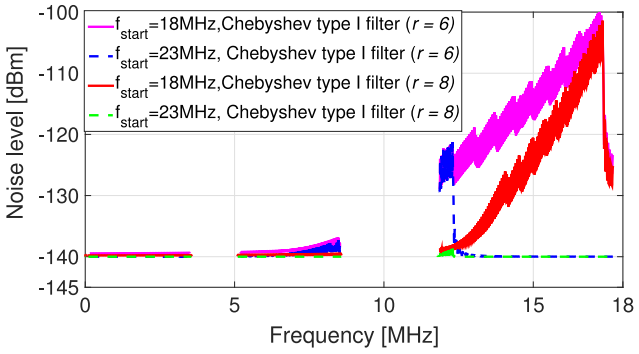

Fig. 10. Total VDSL2 downstream noise with different filter orders and different start frequencies for collocated scenario ($l_1 = 0$ m) and $l_2 = 50$ m. Note that VDSL2 downstream noise does not depend on l_1.

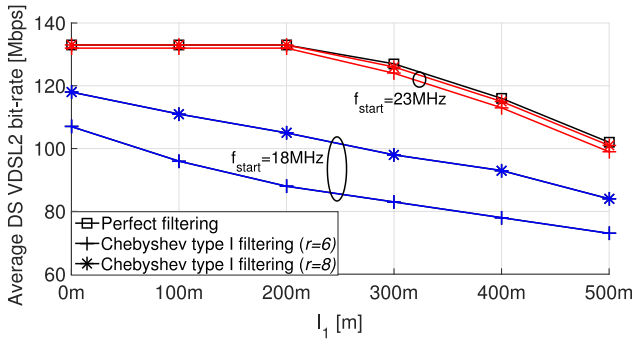

Fig. 11. Average VDSL2 downstream bit-rates for different filter orders, different start frequencies and $l_2 = 50$ m.

VDSL2 CPE (i.e., downstream) for $l_2 = 50$ m, different filter orders, and different G.fast start frequencies. These results indicate that starting G.fast transmission immediately above the VDSL2 in-band (i.e., at around 18 MHz), causes strong noise leakage into VDSL2 downstream bands even under high-order filtering (cf. also the corresponding experiment results in Fig. 1(c) where a large increase in QLN was observed for three different types of VDSL2 modems). As shown in Fig. 11, this strong noise leakage causes substantial VDSL2 downstream bit-rate losses compared to the bit-rates without G.fast interference, e.g., up to 30% for $r = 6$, $l_1 = 500$ m, and $l_2 = 50$ m and increasing further with increasing loop length, reaching up to 40% for $r = 6$, $l_1 = 500$ m, and $l_2 = 200$ m. However, starting G.fast at 23 MHz notably reduces noise leakage, especially for higher order filtering ($r = 8$), keeping the noise levels below -130 dBm/Hz. Furthermore, for VDSL2 downstream transmission NEXT is the dominant noise source due to the collocation of VDSL2 and G.fast users at the CPE side. On the other hand, for VDSL2 upstream transmissions both NEXT and FEXT noise are additionally attenuated over length l_1. For example, in Fig. 12 we see how the total VDSL2 noise at the DSLAM (upstream) decreases as l_1 increases, remaining below -130 dBm/Hz for $l_1 = 500$ m and $l_2 = 50$ m even with a low order Chebyshev type I filter ($r = 6$) and regardless of the spectral separation (i.e., $f_{\text{start}} = 18$ MHz or $f_{\text{start}} = 23$ MHz). Note also that the last VDSL2 downstream band (between 12 MHz and 17.67 MHz) receives the highest noise leakage from G.fast crosstalk signals while the VDSL2 upstream bands receive much lower noise levels. Hence, due to the attenuated G.fast crosstalk signals over length l_1 and the tendentially decreasing noise leakage with decreasing victim tone frequency, the VDSL2 upstream bit-rate losses compared to the interference-free scenario do not exceed 6%. Furthermore, until now we assumed the same 17.7 MHz cut-off frequency for both VDSL2 downstream and upstream transmissions. However, since VDSL2 upstream bands are using frequencies up to 14 MHz (profiles B8-8 and B8-9) in the following we consider a 14 MHz cut-off frequency for VDSL2 upstream receive filters instead.[7]

Fig. 13 shows the total VDSL2 upstream noise for different cut-off frequencies and different spectral separations, i.e., G.fast start frequencies. These results indicate that a 14 MHz cut-off frequency results in substantially reduced VDSL2 upstream noise and therefore the (worst-case) downstream crosstalk represents the main determining factor for selecting the required spectral separation. Fig. 14 shows the total G.fast noise at the CPE side (i.e., DS) for different filter orders, different start frequencies, and for a network scenario where $l_1 = 0$ m, and $l_2 = 50$ m. We see that in order to guarantee noise levels below -130 dBm/Hz G.fast downstream transmission should start above 23 MHz assuming high order filtering ($r = 8$). Note that this selection is experimentally confirmed in Section 2 and is supported by the intuition that it avoids aliasing in the third downstream band, i.e., it is specific for the selected VDSL2 bandplan (with a downstream band between 12 MHz and 17.66 MHz), a popular bandplan in practice.

[7] The VDSL2 bandplan B8-11 allows for an even smaller cut-off frequency (e.g., 12 MHz) for VDSL2 upstream receive filters, implying that the expected noise leakage from G.fast would further decrease.

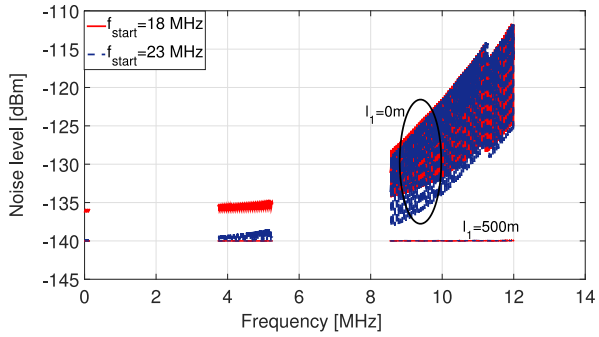

Fig. 12. Total VDSL2 upstream noise for Chebyshev type I filtering ($r = 6$), $l_2 = 50$ m, and different l_1.

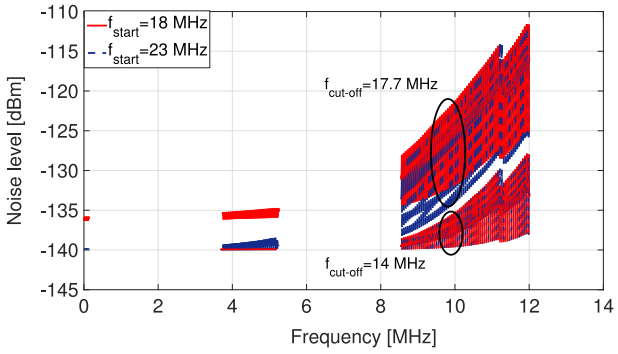

Fig. 13. Total VDSL2 upstream noise for different cut-off frequencies (f_{start}), different G.fast start frequencies (f_{start}), Chebyshev type I filtering ($r = 6$), and collocated scenario ($l_1 = 0$ m) with $l_2 = 50$ m.

Although the selection of non-overlapping spectra mitigates mutual interference it does incur losses in G.fast bit-rates especially on longer loops (i.e., high values of l_2) where high frequencies cannot be used due to the strong insertion loss. Fig. 15 shows average G.fast downstream bit-rates for $l_2 = 200$ m, different G.fast start frequencies, and different filter orders. The bit-rate curves indicate that the G.fast losses compared to the completely overlapped spectrum ($f_{\text{start}} = 2.2$ MHz) increase as spectral separation increases, reaching up to 23% for $f_{\text{start}} = 23$ MHz and $r = 8$. Similar results are found for G.fast upstream transmission (results omitted). However, note that G.fast upstream transmission receives NEXT over wider VDSL2 downstream bands (according to the used bandplan) and correspondingly the losses are slightly higher, reaching up to 27% for $f_{\text{start}} = 23$ MHz and $r = 8$.

5. Conclusions

We analyzed the coexistence of Very high speed digital subscriber line transceivers 2 (VDSL2) and G.fast when being jointly deployed in the same cable binder. These two digital subscriber line (DSL) technologies use different transmission parameters whi ch results in inter-carrier and inter-symbol interference (ICSI). We derived analytical ICSI models under full and partial symbol alignment that capture the transmission properties of both systems. By example it was shown that neglecting ICSI in simulations can potentially lead to 18% bit-rate overestimation for G.fast users. We also show that lower upstream receive filter cut-off frequencies adapted to the upstream bandplan reduce the required spectral separation with respect to upstream transmission. This leaves the downstream coexistence as the more critical test case.

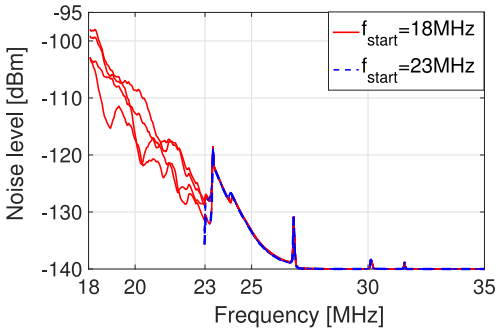

(a) Total G.fast downstream noise ($r = 6$).

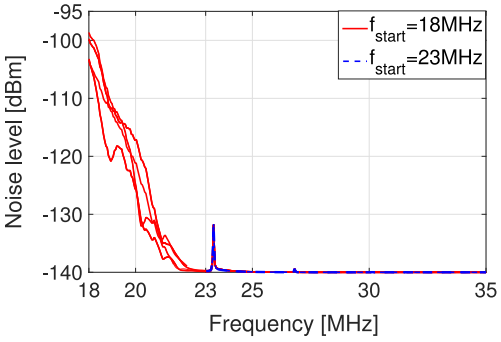

(b) Total G.fast downstream noise ($r = 8$).

Fig. 14. Total G.fast downstream noise for Chebyshev type I filtering of different filter order and for different start frequencies, $l_1 = 0$ m, and $l_2 = 50$ m. Note that additional peak, starting at 23 MHz, arises from attenuated image of the last VDSL2 downstream band.

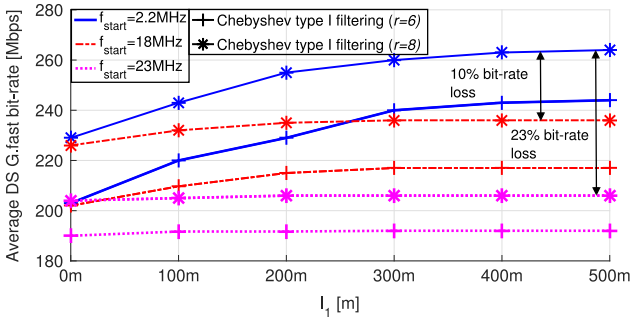

Fig. 15. Average G.fast downstream bit-rates under VDSL2 interference for $l_2 = 200$ m, different filter orders, and different start frequencies.

Furthermore, our simulations of exemplary network scenarios with 8 DSL users show that in order to ensure compatibility with VDSL2 (profile 17a) services, it is sufficient to deactivate G.fast tones below 23 MHz while VDSL2 modems should deploy high order filtering (e.g., a Chebyshev type I filter of order ≥ 8).

Acknowledgment

This work was supported by the Austrian Research Promotion Agency (FFG) under Bridge project no. 855662.

Competing interests

The authors declare that they have no competing interests.

Appendix A. Derivation of VDSL2 crosstalk gains onto G.fast

When VDSL2 interferes with G.fast there are two possible scenarios depending on whether one or two VDSL2 symbols influence a G.fast symbol. We start by analyzing the scenario where one VDSL2 symbol interferes with one G.fast symbol, cf. Fig. 2(a).

A.1. Full alignment scenario

The IDFT of a symbol transmitted by VDSL2 user $u \in \mathcal{U}$ is given as

$$y_n^u = \sum_{k=0}^{2N-1} Y_k^u e^{j\frac{2\pi nk}{2N}} \tag{A.1a}$$

$$= \sum_{k=0}^{N-1} Y_k^u e^{j\frac{2\pi nk}{2N}} + \sum_{k=0}^{N-1} Y_{(2N-k)}^u e^{j\frac{2\pi n(2N-k)}{2N}}, \tag{A.1b}$$

where n and k denote the VDSL2 time and tone indices, respectively, while $2N$ is the IDFT/DFT block size and N is the number of used VDSL2 tones. Note that in (A.1) we use $Y_N^u e^{j\frac{2\pi nN}{2N}} = Y_{2N}^u e^{j\frac{2\pi n2N}{2N}}$. Furthermore, Y_k^u represents the Hermitian symmetric DFT coefficient at tone k [28] while $Y_{(2N-k)}^u = Y_{-k}^u$ corresponds to the negative frequency components of the signal. Assuming Nyquist sampling, G.fast has a higher sampling rate than VDSL2, i.e., $\bar{f}_s > f_s$, where $M = \frac{\bar{f}_s}{f_s}$ is assumed to be an integer. In the following we model a VDSL2 transmitter in the digital domain using M-times oversampling followed by low-pass filtering. Therefore, the VDSL2 signal is first upsampled at the VDSL2 transmitter by a factor of M, i.e.,

$$(y_{\bar{n}}^u)^{\uparrow} = \begin{cases} y_{\frac{\bar{n}}{M}}^u, & \text{if } \bar{n} = mM, m \in [0, 1, \ldots, 2N-1], \\ 0, & \text{otherwise,} \end{cases} \tag{A.2}$$

where $\bar{n}$ denotes the sample index at sampling rate $\bar{f}_s$. VDSL2 and G.fast use different carrier spacings Δf and $\overline{\Delta f}$, where $\overline{\Delta f} > \Delta f$ and $L = \frac{\overline{\Delta f}}{\Delta f}$ which is assumed to be an integer. The number of VDSL2 tones N and G.fast tones $\bar{N}$ are therefore related as $N = \frac{L\bar{N}}{M}$, i.e., $\frac{N}{L} = \frac{\bar{N}}{M}$. As explained later, upsampling admits spectral images of the original VDSL2 spectrum. In order to remove those replicas, a low-pass (anti-image) filter with a passband gain of M is used after upsampling. Therefore, reception for the G.fast (victim) user $\bar{u} \in \bar{\mathcal{U}}$ of the $2\bar{N}$-point upsampled and filtered VDSL2 symbol is given as

$$\bar{Y}_{\bar{k}}^{\bar{u}} = \frac{M}{2\bar{N}} \sum_{u\in\mathcal{U}} \sum_{\bar{n}=0}^{2\bar{N}-1} ((y_{\bar{n}}^u)^{\uparrow} * \bar{q}_{\bar{n}} * h_{\bar{n}}^{\bar{u},u}) e^{-j\frac{2\pi\bar{n}\bar{k}}{2\bar{N}}} \tag{A.3a}$$

$$= \frac{M}{2\bar{N}} \bar{Q}_{\bar{k}} \sum_{u\in\mathcal{U}} H_{\bar{k}}^{\bar{u},u} \sum_{\bar{n}=0}^{\frac{2NM}{L}-1} (y_{\bar{n}}^u)^{\uparrow} e^{-j\frac{2\pi\bar{n}L\bar{k}}{2NM}}, \tag{A.3b}$$

where $*$ denotes the convolution operator, $\bar{q}_{\bar{n}}$ and $\bar{Q}_{\bar{k}}$ are the time and frequency filter taps of the low-pass filter with frequency granularity $\overline{\Delta f}$, and $h_{\bar{n}}^{\bar{u},u}$ and $H_{\bar{k}}^{\bar{u},u}$ are impulse and frequency channel response from user u to user $\bar{u}$ and at time sample $\bar{n}$ and on tone $\bar{k}$, respectively. Using the definition in (A.2) we can rewrite (A.3a) as

$$\bar{Y}_{\bar{k}}^{\bar{u}} = \frac{L}{2N} \bar{Q}_{\bar{k}} \sum_{u\in\mathcal{U}} H_{\bar{k}}^{\bar{u},u} \sum_{\bar{n}=0}^{\frac{2NM}{ML}-1} (y_{M\bar{n}}^u)^{\uparrow} e^{-j\frac{2\pi M\bar{n}L\bar{k}}{2NM}} \tag{A.4a}$$

$$= \frac{L}{2N} \bar{Q}_{\bar{k}} \sum_{u\in\mathcal{U}} H_{\bar{k}}^{\bar{u},u} \sum_{\bar{n}=0}^{\frac{2N}{L}-1} \left(\sum_{k=0}^{N-1} Y_k e^{j\frac{\pi\bar{n}L\bar{d}_1}{N}} + \sum_{k=0}^{N-1} Y_{(2N-k)} e^{j\frac{\pi\bar{n}L\bar{d}_2}{N}} \right), \tag{A.4b}$$

where $(y_{M\bar{n}}^u)^{\uparrow} = y_n$ and y_n^u is defined in (A.1). The two terms in brackets in (A.4a) account for the interference induced from the positive and the negative sides of the VDSL2 spectrum, where $\bar{d}_1 = \frac{k}{L} - \bar{k}$ denotes the spacing between VDSL2 tone k and G.fast tone $\bar{k}$, and $\bar{d}_2 = \frac{(2N-k)}{L} - \bar{k}$ denotes the spacing between VDSL2 tone $2N-k$ and G.fast tone $\bar{k}$. Note that the summation over $\bar{n}$ in Eq. (A.4a) can only go over an integer number of samples. Hence, the DFT size varies between $\lfloor \frac{2N}{L} \rfloor$ and $\lceil \frac{2N}{L} \rceil$ non-zero samples rather than being a constant value for every DFT block, where $\lceil\cdot\rceil$ and $\lfloor\cdot\rfloor$ denote the ceiling and flooring operators, respectively. Therefore, we define the DFT coefficient of user $\bar{u}$ at tone $\bar{k}$ for DFT block size ε as

$$(\bar{Y}_{\bar{k}}^{\bar{u}})^{\varepsilon} = \frac{L}{2N} \bar{Q}_{\bar{k}} \sum_{u\in\mathcal{U}} H_{\bar{k}}^{\bar{u},u} \sum_{\bar{n}=0}^{\varepsilon-1} \left(\sum_{k=0}^{N-1} Y_k^u e^{j\frac{\pi\bar{n}L\bar{d}_1}{N}} + \sum_{k=0}^{N-1} Y_{(2N-k)}^u e^{j\frac{\pi\bar{n}L\bar{d}_2}{N}} \right), \tag{A.5}$$

where $\varepsilon \in \{\lceil \frac{2N}{L} \rceil, \lfloor \frac{2N}{L} \rfloor\}$. From (A.5) we extract contribution from disturber user u to victim user $\bar{u}$ and from disturber tone k on victim tone $\bar{k}$ as:[8]

$$(\bar{Y}_{\bar{k},k}^{\bar{u},u})^{\varepsilon} = \frac{L}{2N} \bar{Q}_{\bar{k}} H_{\bar{k}}^{\bar{u},u} \left(Y_k^u \frac{\sin(\frac{\pi L\bar{d}_1}{2N}\varepsilon)}{\sin(\frac{\pi L\bar{d}_1}{2N})} e^{j\frac{\pi L\bar{d}_1}{2N}(\varepsilon-1)} + Y_{(2N-k)}^u \frac{\sin(\frac{\pi L\bar{d}_2}{2N}\varepsilon)}{\sin(\frac{\pi L\bar{d}_2}{2N})} e^{j\frac{\pi L\bar{d}_2}{2N}(\varepsilon-1)} \right), \tag{A.6}$$

where $(\bar{Y}_{\bar{k}}^{\bar{u}})^{\varepsilon} = \sum_{k=0}^{N-1} \sum_{u\in\mathcal{U}} (\bar{Y}_{\bar{k},k}^{\bar{u},u})^{\varepsilon}$. The squared magnitude of $(\bar{Y}_{\bar{k},k}^{\bar{u},u})^{\varepsilon}$ has the form

$$|(\bar{Y}_{\bar{k},k}^{\bar{u},u})^{\varepsilon}|^2 \propto W^2 + 2WZ\cos(\phi_W + \phi_Z) + Z^2,$$

where $W = |Y_k| \frac{\sin(\frac{\pi L\bar{d}_1}{2N}\varepsilon)}{\sin(\frac{\pi L\bar{d}_1}{2N})}$, $Z = |Y_{2N-k}| \frac{\sin(\frac{\pi L\bar{d}_2}{2N}\varepsilon)}{\sin(\frac{\pi L\bar{d}_1}{2N})}$, $\phi_W = \frac{\pi L\bar{d}_1}{2N}(\varepsilon-1) + \psi_k$, and $\phi_Z = \frac{\pi L\bar{d}_2}{2N}(\varepsilon-1) - \psi_k$, with ψ_k being the phase encoded in DFT coefficients Y_k and Y_{2N-k}, respectively. Furthermore, we express the ICSI coefficients between tones k and $\bar{k}$ and between users u and $\bar{u}$ as $\bar{\gamma}^{\varepsilon}((\bar{k},\bar{u}),(k,u)) = \frac{p_{\bar{k}}^{\bar{u}}}{p_k^u}$. We assume that the ICSI coefficients are user independent (although the transmit PSD levels in (2) can of course still be different among users) and therefore omit the user indexing in the following:

$$\bar{\gamma}^{\varepsilon}(\bar{k},k) = \frac{\mathbb{E}\{|\bar{Y}_{\bar{k},k}^{\varepsilon}|^2\} \frac{1}{R} \frac{1}{\overline{\Delta f}}}{\mathbb{E}\{|Y_k|^2\} \frac{1}{R} \frac{1}{\Delta f}}, \tag{A.7a}$$

$$= \frac{\bar{Q}_{\bar{k}}^2 (H_{\bar{k}})^2}{(\frac{2N}{L})^2} \left(\mathbb{E}\{|Y_k|^2\} \frac{R\overline{\Delta f}}{R\Delta f} \right)^{-1} \cdot \left(\mathbb{E}\{W^2\} + 2\mathbb{E}\{WZ\cos(\phi_W+\phi_Z)\} + \mathbb{E}\{Z^2\} \right) \tag{A.7b}$$

$$= \frac{\bar{Q}_{\bar{k}}^2 (H_{\bar{k}})^2}{(\frac{2N}{L})^2 L} \left(\frac{\sin^2(\frac{\pi L}{2N}\varepsilon\bar{d}_1)}{\sin^2(\frac{\pi L}{2N}\bar{d}_1)} + \frac{\sin^2(\frac{\pi L}{2N}\varepsilon\bar{d}_2)}{\sin^2(\frac{\pi L}{2N}\bar{d}_2)} \right) \tag{A.7c}$$

$$\triangleq \bar{\gamma}^{\varepsilon}(\bar{d}_1, \bar{d}_2), \tag{A.7d}$$

where $\mathbb{E}\{\cdot\}$ is the expectation operator and $R = \bar{R}$, i.e., we assume that both systems use the same reference resistance. Furthermore, to obtain (A.7d) we assume a modulation with symmetrical constellation, $\mathbb{E}\{WZ\cos(\phi_W+\phi_Z)\} = 0$ since $\cos(\varrho+\pi) = -\cos(\varrho)$. From (A.7d) we can show that ICSI coefficients are $\frac{2N}{L}$ periodic with respect to $\bar{k}$. Specifically, the interval $\bar{k} \in [0, \frac{2N}{L}]$ corresponds to

[8] In this step we use the reformulation: $\sum_{n=0}^{N-1} e^{jnx} = \frac{\sin(\frac{1}{2}Nx)}{\sin(\frac{1}{2}x)} e^{\frac{jx(N-1)}{2}}$.

G.fast tones within the VDSL2 spectrum. Due to the ICSI periodicity, G.fast tones outside the VDSL2 spectrum are influenced by ICSI originating from VDSL2 out-of-band spectral images. In order to reduce unwanted spectral images, a low pass filter with taps $\bar{Q}_{\bar{k}}$ has been applied after upsampling to model the out-of-band filter at the VDSL2 transmitter. As mentioned earlier, when $\frac{2N}{L}$ is not an integer we will have alternating DFT block sizes. Therefore, we define the average ICSI coefficients as

$$\bar{\gamma}(\bar{d}_1, \bar{d}_2) = \alpha \bar{\gamma}^{\varepsilon=\lfloor \frac{2N}{L} \rfloor}(\bar{d}_1, \bar{d}_2) + \beta \bar{\gamma}^{\varepsilon=\lceil \frac{2N}{L} \rceil}(\bar{d}_1, \bar{d}_2), \tag{A.8}$$

where $\alpha = \text{mod}(\frac{2N}{L}, 1)$ and $\beta = 1-\alpha$ are the fractions of symbols with length equal to $\lfloor \frac{2N}{L} \rfloor$ and $\lceil \frac{2N}{L} \rceil$, respectively. For overlapping tones we evaluate the limit as

$$\bar{\gamma}(0, \bar{d}_2) = \lim_{\bar{d}_1 \to 0} \bar{\gamma}(\bar{d}_1, \bar{d}_2) \tag{A.9a}$$

$$= \frac{\bar{Q}_{\bar{k}}^2 H_{\bar{k}}^2 (\beta \lceil \frac{2N}{L} \rceil^2 + \alpha \lfloor \frac{2N}{L} \rfloor^2)}{(\frac{2N}{L})^2 L} + \frac{\bar{Q}_{\bar{k}}^2 H_{\bar{k}}^2}{(\frac{2N}{L})^2 L} \Bigg(\beta \frac{\sin^2(\frac{\pi L}{2N} \lceil \frac{2N}{L} \rceil \bar{d}_2)}{\sin^2(\frac{\pi L}{2N} \bar{d}_2)} + \alpha \frac{\sin^2(\frac{\pi L}{2N} \lfloor \frac{2N}{L} \rfloor \bar{d}_2)}{\sin^2(\frac{\pi L}{2N} \bar{d}_2)} \Bigg), \tag{A.9b}$$

where $\bar{\gamma}(\bar{d}_1, 0)$ is defined analogously as in (A.9a).

A.2. Partial alignment scenario

Next, we consider the second symbol alignment scenario (see Fig. 2(b)) where $\varepsilon - \bar{\nu}^\varepsilon$ samples of a VDSL2 symbol and $\bar{\nu}^\varepsilon$ samples of the following VDSL2 symbol affect one G.fast symbol. Two interfering VDSL2 symbols can be represented as truncated versions of the full-length VDSL2 symbols. The truncation is equivalent to a multiplication with a rectangular window in the time domain. Hence, analogously to (A.3a)–(A.6) we obtain the ICSI contributions as follows:

$$\bar{Y}_{\bar{k},k}^{\varepsilon,I} = \frac{M}{2\bar{N}} \sum_{\bar{n}=0}^{2\bar{N}-1} \left((y_{\bar{n}}^{\uparrow} * \bar{q}_{\bar{n}} * h_{\bar{n}}) w_{\bar{n}}^{\bar{\nu}^\varepsilon} \right) e^{-j\frac{2\pi \bar{n} \bar{k}}{2\bar{N}}} \tag{A.10a}$$

$$= \frac{\bar{Q}_{\bar{k}}^2 H_{\bar{k}}^2}{\frac{2N}{L}} \sum_{\bar{n}=0}^{\bar{\nu}^\varepsilon - 1} y_{\bar{n}} e^{-j\frac{2\pi \bar{n} \bar{k} L}{2N}}, \tag{A.10b}$$

$$= \frac{\bar{Q}_{\bar{k}}^2 H_{\bar{k}}^2}{\frac{2N}{L}} \left(Y_k \frac{\sin(\frac{\pi \bar{\nu}^\varepsilon \bar{d}_1 L}{2N})}{\sin(\frac{\pi L \bar{d}_1}{2N})} + Y_{(2N-k)} \frac{\sin(\frac{\pi \bar{\nu}^\varepsilon \bar{d}_2 L}{2N})}{\sin(\frac{\pi L \bar{d}_2}{2N})} \right), \tag{A.10c}$$

$$\bar{Y}_{\bar{k},k}^{\varepsilon,II} = \frac{M}{2\bar{N}} \sum_{\bar{n}=0}^{2\bar{N}-1} \left((y_{\bar{n}}^{\uparrow} * \bar{q}_{\bar{n}} * h_{\bar{n}}) w_{\varepsilon-\bar{n}}^{(\varepsilon-\bar{\nu}^\varepsilon)} \right) e^{-j\frac{2\pi \bar{n} \bar{k}}{2\bar{N}}} \tag{A.10d}$$

$$= \frac{\bar{Q}_{\bar{k}}^2 H_{\bar{k}}^2}{\frac{2N}{L}} \sum_{\bar{n}=\bar{\nu}^\varepsilon}^{\varepsilon - 1} y_{\bar{n}} e^{-j\frac{2\pi \bar{n} \bar{k} L}{2N}}, \tag{A.10e}$$

$$= \frac{\bar{Q}_{\bar{k}}^2 H_{\bar{k}}^2}{\frac{2N}{L}} \Bigg(Y_k \frac{\sin(\frac{\pi \bar{d}_1 L}{2N}(\varepsilon - \bar{\nu}^\varepsilon))}{\sin(\frac{\pi L \bar{d}_1}{2N})} + Y_{(2N-k)} \frac{\sin(\frac{\pi \bar{d}_2 L}{2N}(\varepsilon - \bar{\nu}^\varepsilon))}{\sin(\frac{\pi L \bar{d}_2}{2N})} \Bigg), \tag{A.10f}$$

where $w_{\bar{n}}^{\bar{\nu}^\varepsilon}$ are the coefficients of a rectangular window of integer width $\bar{\nu}^\varepsilon = \lfloor \eta \varepsilon \rfloor$ with $0 \le \eta \le 1$. We assume that VDSL2 symbols are independent. Their contributions to the ICSI coefficients' expected value are therefore additive, yielding the ICSI coefficients for the second symbol alignment scenario:

$$\bar{\gamma}^\varepsilon(\bar{d}_1, \bar{d}_2, \bar{\nu}^\varepsilon) = \frac{\mathbb{E}\{|\bar{Y}_{\bar{k},k}^{\varepsilon,I}|^2\} \frac{R\Delta f}{\bar{R}\Delta \bar{f}}}{\mathbb{E}\{|Y_k + Y_{2N-k}|^2\}} + \frac{\mathbb{E}\{|\bar{Y}_{\bar{k},k}^{\varepsilon,II}|^2\} \frac{R\Delta f}{\bar{R}\Delta \bar{f}}}{\mathbb{E}\{|Y_k + Y_{2N-k}|^2\}}, \tag{A.11a}$$

$$= \frac{\bar{Q}_{\bar{k}}^2 H_{\bar{k}}^2}{(\frac{2N}{L})^2 L} \left(\frac{f^\varepsilon(\bar{d}_1, \bar{\nu}^\varepsilon)}{\sin^2(\frac{\pi L \bar{d}_1}{2N})} + \frac{f^\varepsilon(\bar{d}_2, \bar{\nu}^\varepsilon)}{\sin^2(\frac{\pi L \bar{d}_2}{2N})} \right), \tag{A.11b}$$

where

$$f^\varepsilon(\bar{d}_i, \bar{\nu}^\varepsilon) = \sin^2\left(\frac{\pi \bar{\nu}^\varepsilon \bar{d}_i L}{2N} \right) + \sin^2\left(\frac{\pi \bar{d}_i L}{2N} (\varepsilon - \bar{\nu}^\varepsilon) \right), \tag{A.12}$$

for $0 \le \bar{\nu}^\varepsilon \le \varepsilon$. Average ICSI coefficients are given analogously to (A.8) as

$$\bar{\gamma}(\bar{d}_1, \bar{d}_2, \bar{\nu}^{\varepsilon=\lfloor \frac{2N}{L} \rfloor}, \bar{\nu}^{\varepsilon=\lceil \frac{2N}{L} \rceil}) \tag{A.13}$$

$$= \alpha \bar{\gamma}^{\varepsilon=\lfloor \frac{2N}{L} \rfloor}(\bar{d}_1, \bar{d}_2, \bar{\nu}^{\varepsilon=\lfloor \frac{2N}{L} \rfloor}) + \beta \bar{\gamma}^{\varepsilon=\lceil \frac{2N}{L} \rceil}(\bar{d}_1, \bar{d}_2, \bar{\nu}^{\varepsilon=\lceil \frac{2N}{L} \rceil}).$$

Appendix B. Upper bound on ICSI gain: VDSL2 on G.fast

The definition of ICSI coefficients used in this paper accounts for the worst possible offset $\bar{\nu}^{*\varepsilon}$ for each $\bar{d}_i$, thus, representing an upper bound on ICSI coefficients. For the sake of analytical tractability we derive the ICSI upper bound by relaxing the integer constraint on $\bar{\nu}^\varepsilon$. Furthermore, we independently search for the worst-case offsets for positive and negative frequencies and assume that consecutive symbols are independent. Therefore we maximize ICSI coefficients over two parameters: $\bar{\nu}_1^\varepsilon$ and $\bar{\nu}_2^\varepsilon$. For ε samples long symbols we have the following expression for the worst-case ICSI coefficients

$$\bar{\gamma}^{*\varepsilon}(\bar{d}_1, \bar{d}_2) = \max_{0 \le \bar{\nu}_1^\varepsilon \le \varepsilon} f^\varepsilon(\bar{d}_1, \bar{\nu}_1^\varepsilon) + \max_{0 \le \bar{\nu}_2^\varepsilon \le \varepsilon} f^\varepsilon(\bar{d}_2, \bar{\nu}_2^\varepsilon).$$

The function $f(\bar{d}_i, \bar{\nu}_i^\varepsilon)$ is $\frac{2N}{L}$ periodic with respect to $\bar{k}$. Therefore we define $\bar{\bar{d}}_1 = \frac{k}{L} - (\bar{k}) \text{ mod } \frac{2N}{L}$ and $\bar{\bar{d}}_2 = \frac{2N-k}{L} - (\bar{k}) \text{ mod } \frac{2N}{L}$. Taking the first derivative of $f(\bar{\bar{d}}_i, \bar{\nu}_i^\varepsilon)$ with respect to $\bar{\nu}_i^\varepsilon$ we obtain:

$$\frac{\mathbf{d} f(\bar{\bar{d}}_i, \bar{\nu}_i^\varepsilon)}{\mathbf{d} \bar{\nu}_i^\varepsilon} = 2 \frac{\mathbf{d} B}{\mathbf{d} \bar{\nu}_i^\varepsilon} (-\sin(A)\cos(A) + \sin(B)\cos(B)), \tag{B.1}$$

where $A = \frac{\pi \bar{\nu}_i^\varepsilon \bar{\bar{d}}_i L}{2N}$, $B = \frac{\pi(\varepsilon - \bar{\nu}_i^\varepsilon)\bar{\bar{d}}_i L}{2N}$. There are two cases when (B.1) attains zero: (a) $2A \bmod 2\pi = \theta\pi - 2B \bmod 2\pi$ where $\theta \in \{1, 3\}$ and (b) $2A$=$2B$-C2π. From case (a) it follows that $\bar{\bar{d}}_i = \frac{2N}{L} \varepsilon^{-1} \text{F}$, where F is an uneven integer. However, in this case $f(\bar{\bar{d}}_i, \cdot)$ is constant, i.e., $f(\bar{\bar{d}}_i, \cdot) = f^{*\varepsilon}(\bar{\bar{d}}_i) = 1$. For case (b) and under the assumption that $\bar{\bar{d}}_i \neq 0$ we obtain that (B.1) attains zero when $\tilde{\bar{\nu}}_i^\varepsilon = \frac{\varepsilon}{2} + \frac{CN}{L\bar{\bar{d}}_i}$, where C is a positive integer and we obtain from (A.12)

$$f(\bar{\bar{d}}_i, \tilde{\bar{\nu}}_i^\varepsilon) = \left(\sin\left(\frac{\pi}{2}\bar{\bar{d}}_i\right)\cos\left(\frac{\pi}{2}C\right) - \cos\left(\frac{\pi}{2}\bar{\bar{d}}_i\right)\sin\left(\frac{\pi}{2}C\right) \right)^2 + \left(\sin\left(\frac{\pi}{2}\bar{\bar{d}}_i\right)\cos\left(\frac{\pi}{2}C\right) + \cos\left(\frac{\pi}{2}\bar{\bar{d}}_i\right)\sin\left(\frac{\pi}{2}C\right) \right)^2.$$

Note that for $C = 0$ or even integer $f(\bar{\bar{d}}_i, \tilde{\bar{\nu}}_i^\varepsilon) = 2\sin^2(\frac{\pi \bar{\bar{d}}_i L}{4N}\varepsilon)$ and for $C = 1$ or any other uneven integer $f(\bar{\bar{d}}_i, \tilde{\bar{\nu}}_i^\varepsilon) = 2\cos^2(\frac{\pi \bar{\bar{d}}_i L}{4N}\varepsilon)$. Hence, it is sufficient that in the following analysis we consider $C \in \{0, 1\}$. In order to select the maximum value we use the second derivative test, i.e.,

$$\frac{\mathbf{d}^2 f^\varepsilon(\bar{\bar{d}}_i, \bar{\nu}_i^\varepsilon)}{\mathbf{d}(\bar{\nu}_i^\varepsilon)^2}\Bigg|_{\bar{\nu}_i^\varepsilon = \tilde{\bar{\nu}}_i^\varepsilon} = 4\left(\frac{\mathbf{d} B}{\mathbf{d} \bar{\nu}_i^\varepsilon}\right)^2\Bigg|_{\bar{\nu}_i^\varepsilon = \tilde{\bar{\nu}}_i^\varepsilon} \cos\left(\frac{\pi \bar{\bar{d}}_i L}{2N}\varepsilon\right)\cos(C\pi).$$

The first term is always positive under the assumption that $\bar{\bar{d}}_i \neq 0$. Therefore, we find offsets $\bar{\nu}_i^{*\varepsilon}$ and consequently $f^{*\varepsilon}(\bar{\bar{d}}_i) = f(\bar{\bar{d}}_i, \bar{\nu}_i^{*\varepsilon})$ by analyzing the sign of the cosine terms in different quadrants as done in (6). For overlapping tones we have $\bar{d}_i = 0$ and applying $\lim_{x\to 0} \frac{\sin^2(ax)}{\sin^2(bx)} = \frac{a^2}{b^2}$ in (A.11b) it follows that $\left.\frac{f(\bar{\bar{d}}_i, \bar{\nu}_i^{*\varepsilon})}{\sin^2(\frac{\pi \bar{\bar{d}}_i}{2N})}\right|_{\bar{\bar{d}}_i \to 0} = \varepsilon^2$.

Appendix C. Derivation of G.fast crosstalk gains onto VDSL2

Analyzing the influence of G.fast on VDSL2 we have again two possible scenarios: L entire G.fast symbols influence one VDSL2 symbol or $L-1$ entire and 2 partial G.fast symbols influence one VDSL2 symbol. We begin by analyzing the earlier alignment scenario. The IDFT of a G.fast symbol is given by

$$\begin{aligned}\bar{y}_{\bar{n}} &= \sum_{\bar{k}=0}^{2\bar{N}-1} \bar{Y}_{\bar{k}} e^{j\frac{2\pi \bar{n}\bar{k}}{2N}} \\ &= \sum_{\bar{k}=0}^{\bar{N}-1} \bar{Y}_{\bar{k}} e^{j\frac{2\pi \bar{n}\bar{k}}{2\bar{N}}} + \sum_{\bar{k}=0}^{\bar{N}-1} \bar{Y}_{(2\bar{N}-\bar{k})} e^{j\frac{2\pi \bar{n}(2\bar{N}-\bar{k})}{2\bar{N}}},\end{aligned}$$

where $\bar{Y}_{\bar{k}}$ is the DFT coefficient at tone $\bar{k}$. Due to the M times higher sampling rate, in our model we first downsample the G.fast symbol by factor of M at the VDSL2 receiver. More precisely, we model the VDSL2 receiver in the digital domain as an M-times oversampling analog-to-digital converter followed by low-pass (anti-aliasing) filtering with filter coefficients $\bar{q}_{\bar{n}}$ (including the channel) and a passband gain of one followed by downsampling by a factor of M. Therefore, the filtered G.fast symbol $\bar{\bar{y}}_{\bar{n}} = \bar{y}_{\bar{n}} * \bar{q}_{\bar{n}}$ after downsampling is denoted as $\bar{\bar{y}}_n^{\downarrow} = \bar{\bar{y}}_{nM}$. Since we analyze the effect of a single G.fast symbol, we use zero-padding to obtain the L-times longer VDSL2 interference symbol. The DFT of the padded G.fast symbol is given as

$$\begin{aligned}Y_k &= \frac{1}{2N}\sum_{n=0}^{2N-1} \text{ZeroPad}(\bar{\bar{y}}_n^{\downarrow}) e^{-j\frac{2\pi nk}{2N}}, \\ &= \frac{1}{2N}\sum_{n=0}^{\frac{2N}{L}-1} \bar{\bar{y}}_n^{\downarrow} e^{-j\frac{2\pi nk}{2N}}, \\ &= \frac{1}{2N}\sum_{n=0}^{\frac{2N}{L}-1} \bar{\bar{y}}_{nM} e^{-j\frac{2\pi nk}{2N}}, \\ &= \frac{1}{2N}\sum_{n=0}^{\frac{2N}{L}-1}\sum_{l=0}^{2\bar{N}-1} \bar{q}_l \bar{y}_{(nM-l)} e^{-j\frac{2\pi nk}{2N}}, \\ &= \frac{1}{2N}\sum_{l=0}^{2\bar{N}-1} \bar{q}_l e^{-j\frac{2\pi nk}{2\bar{N}}} \sum_{n=0}^{\frac{2N}{L}-1}\sum_{\bar{k}=0}^{2\bar{N}-1} \bar{Y}_{\bar{k}} e^{j\frac{2\pi \bar{k}ln}{2N}} e^{-j\frac{2\pi nk}{2N}}, \\ &= \frac{\bar{Q}_{\bar{k}}\bar{H}_{\bar{k}}}{2N}\sum_{n=0}^{\frac{2N}{L}-1}\left(\sum_{\bar{k}=0}^{\bar{N}-1} \bar{Y}_{\bar{k}} e^{j\frac{\pi nd_1}{N}} + \sum_{\bar{k}=0}^{\bar{N}-1} \bar{Y}_{2\bar{N}-\bar{k}} e^{j\frac{\pi nd_2}{N}}\right),\end{aligned}$$

where $d_1 = L\bar{k} - k$ denotes the distance between tones $\bar{k}$ and k and $d_2 = L(2\bar{N}-\bar{k}) - k$ denotes the distance between tones $2\bar{N}-\bar{k}$ and k. Equivalently as in Appendix A, DFT coefficients depend on the factor ε, i.e.,

$$\begin{aligned}Y_k^{\varepsilon} = \frac{\bar{Q}_{\bar{k}}\bar{H}_{\bar{k}}}{2N}\Bigg(&\sum_{\bar{k}=0}^{\bar{N}-1} \bar{Y}_{\bar{k}} \frac{\sin(\frac{\pi d_1}{2N}\varepsilon)}{\sin(\frac{\pi d_1}{2N})} e^{j\frac{\pi d_1}{2N}(\varepsilon-1)} \\ &+ \sum_{\bar{k}=0}^{\bar{N}-1} \bar{Y}_{2\bar{N}-\bar{k}} \frac{\sin(\frac{\pi d_2}{2N}\varepsilon)}{\sin(\frac{\pi d_2}{2N})} e^{j\frac{\pi d_2}{2N}(\varepsilon-1)}\Bigg).\end{aligned} \tag{C.1}$$

From (C.1) we can extract the contribution from disturber tone $\bar{k}$ to victim tone k as:

$$\begin{aligned}Y_{k,\bar{k}}^{\varepsilon} = \frac{\bar{Q}_{\bar{k}}\bar{H}_{\bar{k}}}{2N}\Bigg(&\bar{Y}_{\bar{k}} \frac{\sin(\frac{\pi d_1}{2N}\varepsilon)}{\sin(\frac{\pi d_1}{2N})} e^{j\frac{\pi d_1}{2N}(\varepsilon-1)} \\ &+ \bar{Y}_{(2\bar{N}-\bar{k})} \frac{\sin(\frac{\pi d_2}{2N}\varepsilon)}{\sin(\frac{\pi d_2}{2N})} e^{j\frac{\pi d_2}{2N}(\varepsilon-1)}\Bigg),\end{aligned}$$

where $Y_k^{\varepsilon} = \sum_{\bar{k}=0}^{\bar{N}-1} Y_{k,\bar{k}}^{\varepsilon}$. The per-symbol ICSI coefficients $\tilde{\gamma}^{\varepsilon}(\bar{k}, k) = \frac{p_k^u}{p_{\bar{k}}^{\bar{u}}}$ are then calculated analogously as in Appendix A as:

$$\begin{aligned}\tilde{\gamma}^{\varepsilon}(\bar{k}, k) &= \frac{\mathbb{E}\{|Y_{k,\bar{k}}^{\varepsilon}|^2\}\frac{1}{R}\frac{1}{\Delta f}}{\mathbb{E}\{|\bar{Y}_{\bar{k}} + \bar{Y}_{2\bar{N}-\bar{k}}|^2\}\frac{1}{R}\frac{1}{\overline{\Delta f}}} && \text{(C.2a)} \\ &= \frac{\bar{Q}_{\bar{k}}^2\bar{H}_k^2 L}{(2N)^2}\left(\frac{\sin^2(\frac{\pi d_1}{2N}\varepsilon)}{\sin^2(\frac{\pi d_1}{2N})} + \frac{\sin^2(\frac{\pi d_2}{2N}\varepsilon)}{\sin^2(\frac{\pi d_2}{2N})}\right) && \text{(C.2b)} \\ &\triangleq \tilde{\gamma}^{\varepsilon}(d_1, d_2). && \text{(C.2c)}\end{aligned}$$

From (C.2c) we see that the ICSI coefficients are again $\frac{2N}{L}$ periodic with respect to $\bar{k}$. As mentioned in Appendix A, the interval $\bar{k} \in [0, \frac{2N}{L}]$ corresponds to G.fast tones within the VDSL2 spectrum. G.fast tones above the VDSL2 spectrum will be replicated into the VDSL2 spectrum due to the ICSI periodicity. This overlapping effect is called *aliasing* and is reduced by using a low pass filter with DFT coefficients $\bar{Q}_{\bar{k}}$ before downsampling.

The average ICSI coefficients are given as:

$$\tilde{\gamma}(d_1, d_2) = \alpha\tilde{\gamma}^{\varepsilon}(d_1, d_2) + \beta\tilde{\gamma}^{\varepsilon}(d_1, d_2). \tag{C.3}$$

For overlapping tone we again evaluate the limit as

$$\begin{aligned}\tilde{\gamma}(0, d_2) &= \lim_{d_1\to 0} \tilde{\gamma}(\bar{d}_1, \bar{d}_2) && \text{(C.4a)} \\ &= \frac{L\bar{Q}_{\bar{k}}^2\bar{H}_{\bar{k}}^2(\beta\lceil\frac{2N}{L}\rceil^2 + \alpha\lfloor\frac{2N}{L}\rfloor^2)}{(2N)^2} && \text{(C.4b)} \\ &\quad + \frac{L\bar{Q}_{\bar{k}}^2\bar{H}_{\bar{k}}^2}{(2N)^2}\left(\beta\frac{\sin^2(\frac{\pi d_2}{2N}\lceil\frac{2N}{L}\rceil)}{\sin^2(\frac{\pi d_2}{2N})} + \alpha\frac{\sin^2(\frac{\pi d_2}{2N}\lfloor\frac{2N}{L}\rfloor)}{\sin^2(\frac{\pi d_2}{2N})}\right),\end{aligned}$$

where $\tilde{\gamma}(d_1, 0)$ is defined analogously as in (C.4a). Since we assume that G.fast symbols are independent, the average ICSI coefficients including the influence of all L interfering G.fast symbols are given by

$$\check{\gamma}(d_1, d_2) = L\tilde{\gamma}(d_1, d_2).$$

When the G.fast symbols are only partially aligned the ICSI coefficients for $L-1$ fully aligned G.fast symbols are computed according to (C.3), while worst-case ICSI coefficients for partially aligned G.fast symbols are computed similarly as in Appendix A. Thus, we again sum the contributions of two partially aligned symbols and obtain

$$\tilde{\gamma}^{\varepsilon}(d_1, d_2, \nu^{\varepsilon}) = \frac{\bar{Q}_{\bar{k}}^2\bar{H}_{\bar{k}}^2 L}{(2N)^2}\left(\frac{g^{\varepsilon}(d_1, \nu^{\varepsilon})}{\sin^2(\frac{\pi d_1}{2N})} + \frac{g^{\varepsilon}(d_2, \nu^{\varepsilon})}{\sin^2(\frac{\pi d_2}{2N})}\right),$$

where $g^{\varepsilon}(d_i, \nu^{\varepsilon}) = \sin^2\left(\frac{\pi(\varepsilon-\nu^{\varepsilon})d_i}{2N}\right) + \sin^2\left(\frac{\pi\nu^{\varepsilon}d_i}{2N}\right)$ for $0 \leq \nu^{\varepsilon} \leq \varepsilon$ and $i = 1,2$. The shifts ν^{ε} are assumed to be integer values, i.e., $\nu^{\varepsilon} = \lfloor\eta\varepsilon\rfloor$ with $0 \leq \eta \leq 1$. Average ICSI coefficients are given by

$$\begin{aligned}&\tilde{\gamma}(d_1, d_2, \nu^{\varepsilon=\lfloor\frac{2N}{L}\rfloor}, \nu^{\varepsilon=\lceil\frac{2N}{L}\rceil}) \\ &\quad = \alpha\tilde{\gamma}^{\varepsilon=\lfloor\frac{2N}{L}\rfloor}(d_1, d_2, \nu^{\varepsilon=\lfloor\frac{2N}{L}\rfloor}) + \beta\tilde{\gamma}^{\varepsilon=\lceil\frac{2N}{L}\rceil}(d_1, d_2, \nu^{\varepsilon=\lceil\frac{2N}{L}\rceil}).\end{aligned}$$

We see that by replacing $\nu^{\varepsilon} = \frac{\widehat{\nu}^{\varepsilon}}{L}$, $N = \widehat{N}$ and $d_i = L\,\widehat{d}_i$ the same expression as in (A.13) is obtained. Hence, the upper bound on ICSI

coefficients based on the worst-case offset $\nu^{*\varepsilon}$ are obtained as in Appendix A and given by

$$\tilde{\gamma}^*(d_1, d_2) = \alpha\tilde{\gamma}^{*\varepsilon=\lfloor\frac{2N}{L}\rfloor}(d_1, d_2) + \beta\tilde{\gamma}^{*\varepsilon=\lceil\frac{2N}{L}\rceil}(d_1, d_2), \tag{C.5}$$

where $\tilde{\gamma}^{*\varepsilon}(d_1, d_2) = \frac{\bar{Q}_k^2\bar{H}_k^2 L}{(2N)^2}(\rho(d_1) + \rho(d_2))$ with

$$\rho(d_i) = \begin{cases} \dfrac{g^{*\varepsilon}(d_1)}{\sin^2(\frac{\pi d_1}{2N})}, & \text{for } |d_i| \neq 0, \\ \varepsilon^2, & \text{for } |d_i| = 0, \end{cases}$$

and where

$$g^{*\varepsilon}(d_i) = \max_{0\leq\nu^\varepsilon\leq\varepsilon}\{g^\varepsilon(d_i, \nu^\varepsilon)\}$$

$$= \begin{cases} \sin^2(\dfrac{\pi d_i}{2N}\varepsilon), & \text{if } 0 < (\dfrac{\pi|d_i|}{2N}\varepsilon) < \dfrac{\pi}{2}, \\ 2\sin^2(\dfrac{\pi d_i}{4N}\varepsilon), & \text{if } \dfrac{\pi}{2} < (\dfrac{\pi|d_i|}{2N}\varepsilon) \bmod 2 < \dfrac{3\pi}{2}, \\ 2\cos^2(\dfrac{\pi}{2}\dfrac{|d_i|}{L}), & \text{and } 0 \leq (\dfrac{\pi|d_i|}{2N}\varepsilon) \bmod 2 < \dfrac{\pi}{2}, \\ & \text{or } \dfrac{3\pi}{2} < (\dfrac{\pi|d_i|}{2N}\varepsilon) \bmod 2 < 2\pi, \\ 1, & \text{if } |d_i| = F2N\varepsilon^{-1} \\ & \text{where } F \text{ is uneven integer.} \end{cases}$$

Finally, for partial alignment the ICSI coefficients are given as

$$\breve{\tilde{\gamma}}(d_1, d_2) = (L-1)\tilde{\gamma}(d_1, d_2) + \tilde{\gamma}^*(d_1, d_2).$$

References

[1] P. Ödling, T. Magesacher, S. Höst, P. Börjesson, M. Berg, E. Areizaga, The fourth generation broadband concept, IEEE Commun. Mag. 47 (1) (2009) 62–69.
[2] ITU-T, Fast access to subscriber terminals (G.fast) — Physical layer specification, Recommendation G.9701, Dec. 2014.
[3] ITU-T, Fast access to subscriber terminals (G.fast) — Power spectral density specification, Recommendation G.9700, Apr. 2014.
[4] M. Kuipers, F. Chu, Flexible start frequencies and PSD shaping, ITU-T SG15/Q4a Contribution, 2013-05-Q4-069, May 2013.
[5] M. Tilocca, F. Marigliano, T. Starr, H. Mariotte, J. Guy, D. Tjernberg, B. Wang, G. Clerckx, Multi-operators requirements for G.fast, ITU-T SG15/Q4a Contribution, 2012-05-4A-033, May 2012.
[6] L. Humphrey, A. Mohsin, Immunity of VDSL2 to out of band interference from G.fast, ITU-T SG15/Q4a Contribution, 2014-10-Q4-027, Oct. 2014.
[7] V.M.K. Chan, W. Yu, Multiuser spectrum optimization for discrete mutltitone systems with asynchronous crosstalk, IEEE Trans. Signal Process. 55 (11) (2007) 5425–5435.
[8] R.B. Moraes, P. Tsiaflakis, M. Moonen, Intercarrier interference in DSL networks due to asynchronous DMT transmission, in: IEEE International Conference on Acoustics, Speech and Signal Processing, ICASSP, 2013, pp. 4678–4682.
[9] S. Schelstraete, Frequency domain crosstalk canceling between VDSL2 systems with different symbol rates, in: IEEE Sensor Array and Multichannel Signal Processing Workshop, SAM, 2010, pp. 221–224.
[10] F. Mazzenga, W. Utschick, Coexistence of G.fast and VDSL in FTTdp and FTTC Deployments, in: 23rd European Signal Processing Conference, EUSIPCO, 2015. pp. 1103–1107.
[11] L. Marijanovic, S. Schwarz, M. Rupp, Intercarrier interference of multiple access UFMC with flexible subcarrier spacings, in: Proceedings of the 25th European Signal Processing Conference, EUSIPCO, 2017, pp. 918–922.
[12] M. Nemati, H. Arslan, Low ICI symbol boundary alignment for 5G numerology design, IEEE Access 6 (2018) 2356–2366.
[13] W.S. Hou, B.S. Chen, ICI cancellation for OFDM communication systems in time-varying multipath fading channels, IEEE Trans. Wirel. Commun. 4 (2005) 2100–2110.
[14] H. Steendam, M. Moeneclaey, Analysis and optimization of the performance of OFDM on frequency-selective time-selective fading channels, IEEE Trans. Commun. 47 (12) (1999) 1811–1819.
[15] Y. Li, L.J. Cimini, Bounds on the interchannel interference of OFDM in time-varying impairments, IEEE Trans. Commun. 49 (3) (2001) 401–404.
[16] M. García, C. Oberli, Intercarrier Interference in OFDM: A general model for Transmissions in mobile environments with imperfect synchronization, EURASIP J. Wirel. Commun. Netw. 2009 (1) (2009) 1–11.
[17] C. Oberli, ML-based tracking algorithms for MIMO-OFDM, IEEE Trans. Wirel. Commun. 6 (7) (2007) 2630–2639.
[18] X. Liu, D. He, M. Jia, 5G-based wideband cognitive radio system design with cooperative spectrum sensing, Phys. Commun. 25 (P1) (2017) 539–545.
[19] X. Liu, D. He, W. Lu, F. Li, Bandwidth allocation-based simultaneous cooperative spectrum sensing and energy harvesting for multicarrier cognitive radio, Phys. Commun. 25 (P1) (2017) 284–291.
[20] F. Schaich, T. Wild, R. Ahmed, Subcarrier spacing — how to make use of this degree of freedom, in: 2016 IEEE 83rd Vehicular Technology Conference, VTC Spring, 2016, pp. 1–6.
[21] M. Sliskovic, Carrier and sampling frequency offset estimation and correction in multicarrier systems, in: IEEE Global Telecommunications Conference, GLOBECOM, Vol. 1, 2001, pp. 285–289.
[22] M. Park, K. Ko, B. Park, D. Hong, Effects of asynchronous MAI on average SEP performance of OFDMA uplink systems over frequency-selective Rayleigh fading channels, IEEE Trans. Commun. 58 (2) (2010) 586–599.
[23] S. Drakulić, M. Wolkerstorfer, D. Statovci, Coexistence analysis of asynchronous digital subscriber lines with different sampling rate and carrier frequency spacing, in: IEEE Global Communications Conference, GLOBECOM, 2014, pp. 2234–2239.
[24] M. Wolkerstorfer, D. Statovci, S. Drakulić, Maintaining harmony in the vectoring xDSL family by spectral coordination, in: 49th Asilomar Conference on Signals, Systems and Computers, 2015, pp. 1739–1743.
[25] ITU-T, Physical layer management for digital subscriber line (DSL) transceivers, G.997.1, Jun. 2012.
[26] D. Van Bruyssel, J. Maes, Considerations regarding the choice of the duplexing scheme, ITU-T SG15/Q4a Contribution, 11RV-025, Nov. 2011.
[27] ITU-T, Very high speed digital subscriber line transceivers 2 (VDSL2), Recommendation G.993.2, Jan. 2015.
[28] P. Golden, H. Dedieu, K. Jacobsen (Eds.), Fundamentals of DSL Technology, CRC Press, Boca Raton, Florida, 2005.

Sanda Drakulić received her B.Sc. degree in Telecommunications and Informatics from the Faculty of Electrical Engineering and Computing in Zagreb, Croatia, in 2008, her first M.Sc. degree in Telecommunications engineering from the Polytechnic University of Milan in 2010, and her second M.Sc. degree in Telecommunications and Informatics from the Faculty of Electrical Engineering and Computing in Zagreb, in 2012. The research topics of her M.Sc. theses were security and power optimization in optical networks. From 2012 until 2015, Ms. Drakulić worked as a researcher at t he Telecommunications Research Center Vienna (FTW), Austria. There she was working on topics related to G.fast, the fourth-generation DSL standard. In 2015 she joined the Institute of Telecommunications at TU Wien, where she received her PhD degree in 2017. Her current research is focused on interference mitigation and cancelation techniques for G.fast and mixed G.fast/legacy DSL scenarios, channel modeling for mixtures of xDSL technologies, and the analysis of deployment strategies for G.fast systems.

Martin Wolkerstorfer received the Dipl.-Ing. degree in electrical engineering from Graz University of Technology, Austria, in 2007, and the Dr. techn. degree from Vienna University of Technology, Austria, in 2012. From 2008 to 2015 he worked as researcher (senior researcher since 2012) and project leader at the Telecommunications Research Center Vienna (FTW) in the field of signal and information processing for wired communication networks. During 2010 and 2012 he was a one-month visiting researcher at the Signal Processing Laboratory, KTH Stockholm (Sweden) and the Department of Electrical Engineering (ESAT-SCD), KU Leuven (Belgium), respectively. He (co-)authored over 30 scientific publications in international journals, conference proceedings, and edited books. In 2015 he joined the Institute of Telecommunications at Vienna University of Technology. His current research interests include the modeling, evaluation, and optimization of broadband wireline access (xDSL) and Powerline Communication (PLC) networks, as well as the application of optimization and game theory for interference management.

Driton Statovci received the Inxh. i dipl. degree (equivalent to a masters degree) in the field of Telecommunications and Informatics from University of Prishtina, Prishtina, Kosova in 1996. He received the Ph.D. degree (passed with distinction) from Vienna University of Technology, Austria, on the topic of adaptive resource allocation for multi-user digital subscriber lines systems, in 2005. From 2000 until 2002 he worked at Ahead Communications Systems AG as a design engineer and project manager, where he designed and implemented communication systems for transmitting data and voice over digital

subscriber line (DSL) access networks. From 2002 until 2015 he worked at Telecommunications Research Center Vienna (FTW) in the field of signal and information processing for wireline communications, where he held different positions such as Researcher (until 2005), Senior Research (from 2005), Project Manager (from 2009), and Wireline Communication group leader (from 2011). In 2015 he joined the Institute of Telecommunications at Vienna University of Technology as project assistant. His research interests include: signal processing and energy-efficient wireline systems, interference mitigation and cancellation in DSL systems, and application of optimization techniques in communication systems.